Monthly Notices of the ROYAL ASTRONOMICAL SOCIETY

MNRAS **504,** 920–925 (2021) doi:10.1093/mnras/stab1004
Advance Access publication 2021 April 10

New X-ray observations of the hot subdwarf binary HD 49798/RX J0648.0–4418

S. Mereghetti [1]★ F. Pintore [2]★ T. Rauch,[3] N. La Palombara [1] P. Esposito,[4] S. Geier,[5] I. Pelisoli [5,6] M. Rigoselli [1] V. Schaffenroth[5] and A. Tiengo [4]

[1]*INAF – IASF Milano, Via A. Corti 12, I-20133 Milano, Italy*
[2]*INAF – IASF Palermo, Via U. La Malfa 153, I-90146 Palermo, Italy*
[3]*Institute for Astronomy and Astrophysics, Kepler Center for Astro and Particle Physics, Eberhard Karls University, Sand 1, D-72076 Tübingen, Germany*
[4]*Scuola Universitaria Superiore IUSS Pavia, Piazza della Vittoria 15, I-27100 Pavia, Italy*
[5]*Institut für Physik und Astronomie, Universität Potsdam, Haus 28, Karl-Liebknecht-Str 24/25, D-14476 Potsdam-Golm, Germany*
[6]*Department of Physics, University of Warwick, Coventry, CV4 7AL, UK*

Accepted 2021 April 7. Received 2021 April 7; in original form 2021 February 23

ABSTRACT

HD 49798/RX J0648.0–4418 is the only confirmed X-ray binary in which the mass donor is a hot subdwarf star of O spectral type and, most likely, it contains a massive white dwarf ($1.28 \pm 0.05\,M_{\odot}$) with a very fast spin period of 13.2 s. Here, we report the results of new *XMM–Newton* pointings of this peculiar binary, carried out in 2018 and in 2020, together with a reanalysis of all the previous observations. The new data indicate that the compact object is still spinning-up at a steady rate of $(-2.17 \pm 0.01) \times 10^{-15}\,s\,s^{-1}$, consistent with its interpretation in terms of a young contracting white dwarf. Comparison of observations obtained at similar orbital phases, far from the ecplise, shows evidence for long-term variability of the hard (>0.5 keV) spectral component at a level of ∼(70 ± 20) per cent, suggesting the presence of time-dependent inhomogeneities in the weak stellar wind of the HD 49798 subdwarf. To investigate better the soft spectral component that dominates the X-ray flux from this system, we computed a theoretical model for the thermal emission expected from an atmosphere with element abundances and surface gravity appropriate for this massive white dwarf. This model gives a best fit with effective temperature of $T_{eff} = 2.25 \times 10^5$ K and an emitting area with a radius of ∼1600 km, larger than that found with blackbody fits. This model also predicts a contribution of the pulsed emission from the white dwarf in the optical band significantly larger than previously thought and possibly relevant for optical variability studies of this system.

Key words: subdwarfs – white dwarfs – X-rays: binaries.

1 INTRODUCTION

HD 49798/RX J0648.0–4418 is the only known accreting X-ray binary in which the mass donor belongs to the class of hot subdwarf stars (Heber 2016). This binary, likely the outcome of a common envelope stage, is relevant in the context of evolutionary models of intermediate-mass stars, possibly leading to the formation of millisecond pulsars or Type Ia supernovae (Wang & Han 2010; Brooks, Kupfer & Bildsten 2017; Wu & Wang 2019). It is also interesting because, through the study of its X-ray emission, it offers the possibility to obtain some information on the weak stellar wind of the hot subdwarf (Mereghetti & La Palombara 2016; Krtička et al. 2019).

HD 49798/RX J0648.0–4418 is composed of a compact object spinning at P = 13.2 s and a subdwarf star of O spectral type (Kudritzki & Simon 1978; Israel et al. 1997; Mereghetti et al. 2011). The orbital period, determined through optical spectroscopy since early observations of HD 49798, is 1.55 d (Thackeray 1970). The masses of the two stars are well constrained by the measurement of the optical and X-ray mass functions, the system inclination being derived from the duration of the X-ray eclipse: the compact object has a mass of $1.28 \pm 0.05\,M_{\odot}$ and is most likely a white dwarf, while the mass of HD 49798 is $1.50 \pm 0.05\,M_{\odot}$ (Mereghetti et al. 2009). The most recent parallax obtained with *Gaia* EDR3 corresponds to a distance of 521 ± 14 pc (Brown et al. 2020).

Contrary to the majority of X-ray binaries, which are transient or highly variable, RX J0648.0–4418 is a persistent X-ray source: a luminosity of $\sim 10^{32}$ erg s^{-1} was seen in all observations, that now span almost 30 yr. With a radius of $\sim 1 R_{\odot}$, HD 49798 underfills its Roche lobe, but it is one of the few hot subdwarfs with strong evidence for a stellar wind (Hamann et al. 1981; Hamann 2010). The most recent estimate, obtained through the modeling of high-resolution UV/optical spectra, yields a mass-loss rate of $2.1 \times 10^{-9}\,M_{\odot}\,yr^{-1}$ and a wind terminal velocity of 1570 km s^{-1} (Krtička et al. 2019). With these stellar wind parameters, the observed X-ray luminosity is consistent with that expected from accretion on to a massive white dwarf (Mereghetti et al. 2009, 2011).

Besides the low X-ray luminosity, much smaller than that expected if the accreting object were a neutron star, there are other arguments that support the presence of a white dwarf in this system. Most of the X-ray flux is emitted in a very soft and strongly pulsed thermal component, well fitted by a blackbody with temperature of kT∼30 eV and an emitting radius of ∼30 km (Mereghetti et al. 2016). These dimensions are consistent with those of a hotspot on the surface of a

★ E-mail: sandro.mereghetti@inaf.it (SM); fabio.pintore@inaf.it (FP)

Table 1. Log of the *XMM–Newton* observations of HD 49798.

Date	Obs. ID	Start (MJD)	Stop (MJD)	Exposure pn/MOS (ks)	Orbital phase
2002 May 3	0112450301	52397.46	52397.55	4.5/7.2	0.45–0.48
2002 May 4	0112450401	52397.98	52398.06	1.4/5.4	0.78–0.81
2002 May 4	0112450501	52398.56	52398.59	0.6/2.5	0.17–0.16
2002 Sep 17	0112450601	52534.58	52534.72	6.9/11.9	0.06–0.11
2008 May 10	0555460201	54596.90	54597.38	36.7/43.0	0.56–0.87
2011 May 2	0671240901	55683.55	55683.76	17.0/18.3	0.70–0.82
2011 Aug 18	0671241001	55791.88	55792.07	15.0/16.4	0.69–0.80
2011 Aug 20	0671241101	55793.46	55793.62	11.8/14.1	0.72–0.80
2011 Aug 25	0671241201	55798.04	55798.27	18.0/19.2	0.67–0.81
2011 Sep 3	0671241301	55807.35	55807.54	15.0/16.4	0.69–0.80
2011 Sep 8	0671241401	55811.10	55812.19	15.0/16.4	0.70–0.80
2013 Nov 10	0721050101	56605.80	56606.25	37.9/39.1	0.60–0.86
2014 Oct 18	0740280101	56948.37	56948.71	27.1/29.1	0.95–0.15
2018 Nov 8	0820220101	58430.46	58430.92	34.3/40.9	0.56–0.85
2020 Feb 27	0841270101	58906.31	58906.81	37.3/45.4	0.03–0.35

white dwarf, but are too large for a neutron star. This emitting radius could be reconciled with a neutron star only if the X-ray emission comes from the whole (or a large part of the) star surface, but this is at variance with the very high pulsed fraction of the soft X-ray pulse profile (∼65 per cent).

The steady long-term spin-up of RX J0648.0–4418, at a rate of $\dot{P} = -2.15 \times 10^{-15}$ s s^{-1}, is difficult to explain by accretion torques (Mereghetti et al. 2016). On the other hand, Popov et al. (2018) showed that it is consistent with that caused by the radial contraction of a young white dwarf with age of a few millions years. Such a small age is in agreement with the evolutionary models that account for the properties of this binary. Finally, we note that population synthesis simulations of hot subdwarf binaries predict that those hosting white dwarfs greatly outnumber those with a neutron star (Yungelson & Tutukov 2005; Wu et al. 2018).

To continue our long-term monitoring of this unique X-ray binary, we observed it with *XMM–Newton* in 2018 and 2020. Here, we present the results of these new observations, complemented by a reanalysis of all the previous data, including the first spectral fits with a white dwarf atmosphere model applied to this system.

2 DATA ANALYSIS AND RESULTS

XMM–Newton observed RX J0648.0–4418 for ∼34 ks on 2018 November 8 and for ∼37 ks on 2020 February 27. We use the data obtained with the EPIC instrument, which consists of one pn and two MOS cameras (Strüder et al. 2001; Turner et al. 2001). As in all the previous observations, the pn and MOS cameras were operated in full-frame mode, giving time resolutions of 73 ms and 2.6 s, respectively.

To compare properly the new observations with the previous ones, we processed all the available *XMM–Newton* data using SAS v.16.1 and the most recent calibration files. We filtered out time intervals with high background and selected single- and double-pixels events for the pn (PATTERN ≤ 4), and single- and multiple-pixels events for the MOS (PATTERN ≤ 12). The resulting exposure times are given in Table 1. Source and background events were extracted from circular regions with radii of 30 and 60 arcsec, respectively.

For the timing analysis, we used also the *ROSAT* data obtained on 1992 November 11. We selected the counts obtained with the PSPC instrument in the energy range 0.1–0.5 keV, from a source region with radius of 1 arcmin.

Table 2. Phase-coherent timing solution valid in the 48937.75–58761.81 MJD range.

Parameter	Value	Units
Right ascension	$6^h\,48^m\,4\overset{s}{.}7$	J2000
Declination	$-44^\circ\,18'\,58\overset{''}{.}4$	J2000
Orbital period	1.547666	d
A_X sin i	9.78646	light-s
T^*	43962.017[a]	MJD
ν_0	0.075848091873(12)	Hz
$\dot{\nu}$	$1.250(7) \times 10^{-17}$	Hz s^{-1}
P_0	13.184247295(2)	s
$\dot{P}$	$-2.17(1) \times 10^{-15}$	s s^{-1}
T_0	55793.4827567	MJD

Note. [a] Due to a typo, this parameter was incorrectly reported in table 2 of Mereghetti et al. (2016). With this definition of T^* the eclipse occurs at orbital phase 0.75.

For all data sets, the times of arrival of the events were corrected to the Solar system barycentre using the source coordinates given in Table 2.

2.1 Timing analysis results

The source pulsations at 13.2 s are cleary visible in the 2018 and 2020 data. The spin periods measured in these new observations are consistent with those predicted by the ephemeris reported in Mereghetti et al. (2016), which were derived from a phase-coherent timing of all the data obtained before 2015. Therefore, we included the new data in the phase-coherent analysis. Briefly, this consists in deriving the time of arrivals of a fiducial phase of the pulse profile measured in the different observations and, after correcting for the effect of orbital motion, fitting them with a quadratic function $\phi(t) = \phi_0(t) + \nu_0(t - T_0) + 0.5\dot{\nu}(t - T_0)^2$. The phases were determined by fitting a sinusoidal function to the 0.15–0.5 keV pulse profiles measured in time intervals of 2000 s. This procedure was done iteratively, starting from the most closely spaced observations, and progressively including the other ones, as the improved timing parameters allow to mantain phase coherence. The orbital parameters were kept fixed at the values of Table 2.

Our final solution provided a good fit ($\chi^2_\nu = 1.21$ for 44 degrees of freedom) and a highly significant quadratic term with the parameters

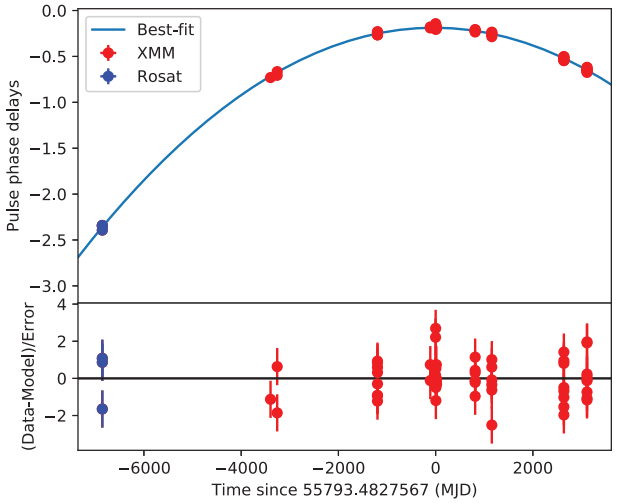

Figure 1. Timing solution (in units of phase, the solid blue line) for ∼28 yr of observations of HD 49798/RX J0648.0–4418. The residuals of the best-fitting model are presented in the bottom panel.

given in Table 2. The best fit and its residuals are shown in Fig. 1. This timing solution is consistent with that of Mereghetti et al. (2016), but, because of the longer baseline, it has smaller uncertainties on the best-fitting parameters.

To search for long-term variability, disentangling the effects related to the orbital phase, we produced background-subtracted light curves folded at the orbital period (Fig. 2). They refer to the soft (0.2–0.5 keV) and hard (0.5–10 keV) energy bands. It can be seen that there is some evidence that the hard X-ray flux in 2020 was slightly lower than in previous observations that covered similar orbital phases. This is indeed confirmed by the spectral analysis described below. The 2020 hard X-ray light curve shows also evidence for some variability on time-scales of few hundreds seconds. In fact a fit with a constant of the data binned at 400 s yields $\chi^2_\nu = 1.66$ for 108 degrees of freedom.

2.2 X-ray emission during the eclipse

The 2018 observation covered the orbital phases around the eclipse of the X-ray pulsar and confirms the presence of significant X-ray emission also when the compact object is occulted by its subdwarf companion, as it was seen in previous eight observations (Mereghetti et al. 2009, 2013). To investigate possible long-term variability of the emission during the eclipse, we extracted EPIC-pn images (in the 0.3–4.5 keV range) in a time interval of 4300 s (the eclipse duration measured in Mereghetti et al. 2013) centred at phase 0.75 and carried out source detections using the SAS task *edetect_chain*. HD 49798 was detected in all the nine images, with count rates consistent with a constant value of 0.048 ± 0.002 counts s^{-1} ($\chi^2_\nu = 1.44$ for 8 degrees of freedom).

We then produced a pn and an MOS spectrum of the eclipse emission by stacking all the source spectra of the individual observations, extracted from the above orbital phase interval. These two spectra were fit simultaneously using the sum of three thermal plasma emission models (vapec in XSPEC) with abundances fixed to the most recent values found for HD 49798 (see table 2 of Krtička et al. 2019). The resulting temperatures of 0.15, 0.9, and 6 keV, and the corresponding model normalizations, were consistent with those found by Mereghetti & La Palombara (2016). Under the assumption that the X-ray flux seen during the eclipse is due to intrinsic emission

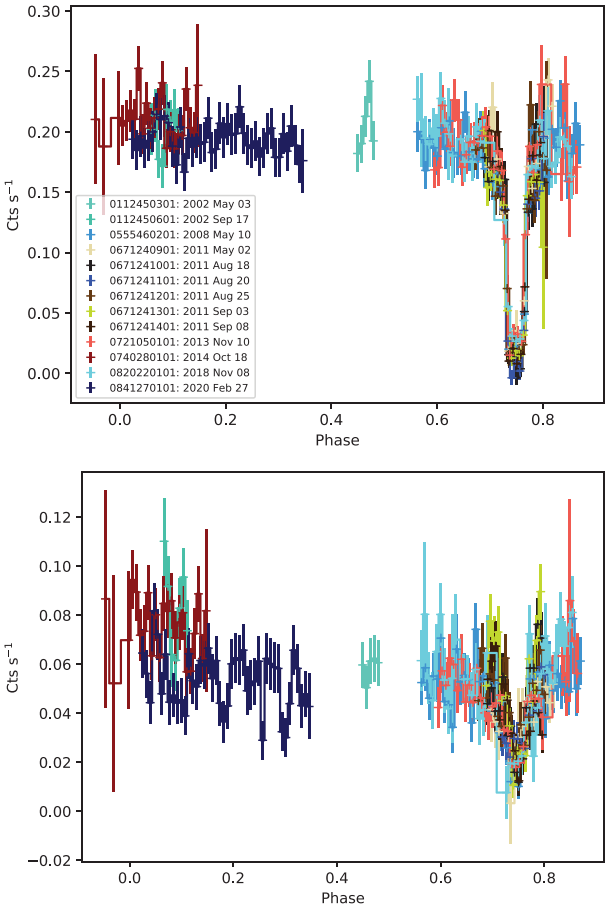

Figure 2. Light curves folded at the orbital period in the soft (0.2–0.5 keV, top) and hard (0.5–10 keV, bottom) energy ranges. The eclipse occurs at phase 0.75. The time bin is 1000 s.

from HD 49798, and thus present at all orbital phases, we included this best-fitting eclipse model as a fixed component in all the subsequent spectral fits discussed below.

2.3 Variability in the hard X-ray component

The 2020 observation provided the first data set with a long exposure time at orbital phases far from the eclipse, which were covered only marginally by previous *XMM–Newton* pointings. For a first analysis of these data and to facilitate the comparison with previous results, we adopted a blackbody plus power-law model and we concentrated on a comparison with the 2014 observation, which covered similar orbital phases.

Separate fits to the 2014 and 2020 spectra, in the 0.3–10 keV range, gave consistent values for the blackbody component, but different best-fitting parameters for the power law, indicating a lower flux in 2020. Therefore, we fitted the 2014 and 2020 pn spectra simultaneously, imposing common values for all the parameters except for the power-law normalization. This resulted in a good fit ($\chi^2_\nu = 1.15$ for 167 degrees of freedom) with 0.3–10 keV fluxes of the power law component of $(1.7 \pm 0.2) \times 10^{-13}$ erg cm^{-2} s^{-1} in 2014 and $(1.0 \pm 0.1) \times 10^{-13}$ erg cm^{-2} s^{-1} in 2020. These flux values confirm the evidence for the variability seen in the hard X-ray light curves of Fig. 2. All the other spectral parameters were consistent with those obtained from the sum of all the data taken before 2015

(Mereghetti et al. 2016), although they had larger uncertainties due to their lower counting statistics.

2.4 The soft thermal component

Since with the new observations we found no evidence for long-term variability in the soft thermal component, we performed a spectral analysis using the spectra obtained by stacking all the available observations. In the following, we present the results obtained with the EPIC-pn spectra,[1] corresponding to a total exposure time of 170 ks. In addition to fits with the usual blackbody plus power law model, we also explored a more physically motivated scenario, replacing the blackbody component with a white dwarf atmosphere model that we computed specifically for this source.

The effects of an atmosphere on the emerging thermal radiation depend on many parameters, including elemental composition and surface gravity, but it is impossible to constrain all of them with the limited spectral resolution and narrow bandwidth of the current data. Therefore, we explored only a single model that we computed assuming a surface gravity of $\log g = 9$ (appropriate for this massive white dwarf) and a composition based on the abundances measured for HD 49798 (Krtička et al. 2019). This choice for the abundances is based on the hypothesis that the white dwarf surface, or at least the regions where matter accretes and that are responsible for the X-ray emission, are covered by matter coming from the companion star.

To model stellar spectra in the relevant $T_{\rm eff}$ and $\log g$ ranges, non-local thermodynamic equilibrium (NLTE) model atmospheres are mandatory. Thus, we employed the Tübingen NLTE Model-Atmosphere Package[2] (Werner et al. 2003; Werner, Dreizler & Rauch 2012) to calculate plane-parallel and chemically homogeneous atmospheres in hydrostatic and radiative equilibrium. We considered opacities of H, He, C, N, O, Fe, and Ni. The atomic data were taken from the Tübingen Model-Atom Database (TMAD) and, for Fe and Ni, calculated with our Iron Opacity and Interface program (IrOnIc), which uses a statistical approach with so-called super levels and super lines (Rauch & Deetjen 2003) based on Kurucz's line lists[3] (Kurucz 2009, 2011) and Opacity Project data[4] (Seaton et al. 1994). We adopted the abundances given by the following normalized mass fractions: H (8.045×10^{-2}), He (9.134×10^{-1}), C (2.337×10^{-4}), N (3.431×10^{-3}), O (1.239×10^{-4}), Fe (2.168×10^{-3}), and Ni (1.817×10^{-4}). Some examples of the model for different values of the effective temperature are shown in Fig. 3. Due to the presence of many absorption lines and edges, they deviate significantly from blackbody spectra, especially at the shortest wavelengths. This is also illustrated in Fig. 4, which presents an enlarged view of the energy range covered by our X-ray data. In this figure, the theoretical model has been convolved with the instrumental response of the EPIC pn detector, which results in a smearing of the sharp spectral features.

By fitting the pn spectrum with the atmosphere model plus a power law, we could not obtain a unique best-fitting solution. In fact, exploring the whole range of temperatures covered by our model,[5] we found similarly good results with effective temperatures of about 2.2 or 2.9×10^5 K ($\chi^2_\nu = 1.26$ and 1.28, respectively). These fits imply emitting regions more than one hundred times larger than that

[1]We checked that similar results were obtained with the MOS.
[2]http://astro.uni-tuebingen.de/~TMAP
[3]http://kurucz.harvard.edu/atoms.html
[4]http://cdsweb.u-strasbg.fr/topbase/topbase.html
[5]We imposed values of $N_{\rm H} > 10^{20}$ cm^{-2} to avoid convergence of the fits to unreasonable values.

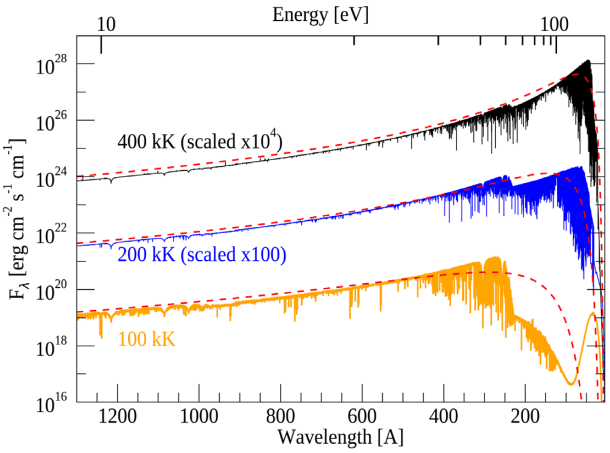

Figure 3. Examples of our white dwarf atmosphere model for effective temperatures of 10^5, 2×10^5, and 4×10^5 K. Note that the two latter have been rescaled by two and four decades for clarity. The red-dashed lines indicate for comparison blackbody models with the corresponding temperatures.

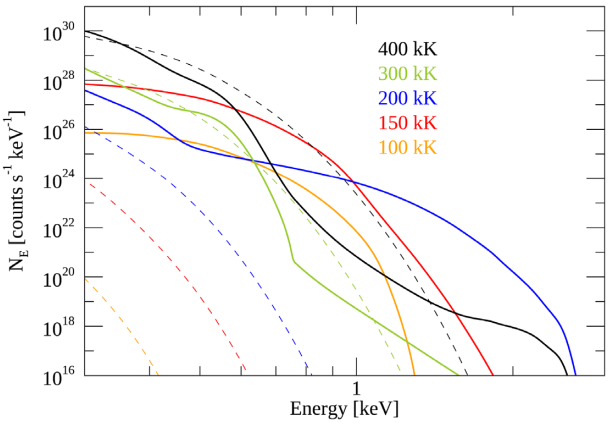

Figure 4. Examples of our white dwarf atmosphere model in the 0.3–3 keV energy range folded through the EPIC pn response. The dashed lines represent blackbody models with the corresponding temperatures.

derived with the blackbody model (see Table 3). Another reasonably good fit, with only a slightly worse $\chi^2_\nu = 1.39$, was found for $T_{\rm eff} = 3.7 \times 10^5$ K.

The reason for these multiple solutions can be qualitatively understood by examining Fig. 4: in the ~0.3–0.6 keV range, where the thermal emission dominates over the power-law component, the atmosphere model has an average spectral slope that varies with temperature in a non-monotonic way. The slope observed in the X-ray data, and well described by a blackbody of $\sim 3.7 \times 10^5$ K, can be well approximated by atmosphere models with different values of $T_{\rm eff}$, also considering the effect of changes in $N_{\rm H}$ and in the power-law parameters (see best-fitting values in Table 3).

The best-fitting to the pn spectrum with an atmosphere of $T_{\rm eff} = 2.25 \times 10^5$ K is shown in Fig. 5. The residuals in the fits, which lead to a χ^2_ν value slightly higher than that obtained with a blackbody, could be reduced by changing the atmosphere metal abundances and/or surface gravity (as well as by allowing some small variations in the eclipse model used to describe the contribution from HD 49798). However, besides increasing the number of free parameters, this would not lead to a unique solution and we believe

Table 3. Spectral results (errors at 90% c.l.).

Model	N_H 10^{20} cm^{-2}	T_{eff} 10^5 K	R[a] (km)	Photon index	F^b_{PL} 10^{-13} erg cm^{-2} s^{-1}	χ^2_ν/degrees of freedom
BB + PL	1 (fixed)	3.65 ± 0.18	41^{+13}_{-10}	1.80 ± 0.06	1.18 ± 0.05	1.16/116
Atm + PL	14.3 ± 1.5	$2.25^{+0.02}_{-0.04}$	1604^{+207}_{-212}	1.75 ± 0.09	1.23 ± 0.06	1.26/116
Atm + PL	8.5 ± 0.8	2.94 ± 0.01	397 ± 32	1.66 ± 0.09	1.20 ± 0.06	1.28/116
Atm + PL	6.3 ± 1.5	$3.73^{+0.04}_{-0.19}$	66^{+26}_{-9}	1.92 ± 0.06	1.22 ± 0.05	1.39/116

Notes. [a]Emission radius for d = 521 pc.
[b]Unabsorbed flux of power law component in the 0.3–10 keV energy range.

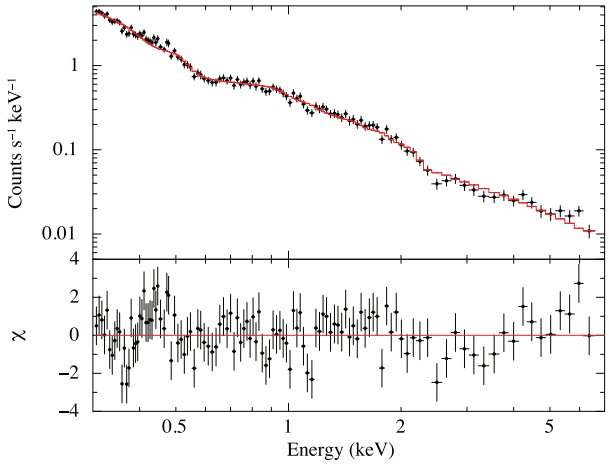

Figure 5. Best fit (top) and residuals (bottom) of the total pn spectrum with a power law plus atmosphere model with $T_{eff} = 2.25 \times 10^5$ K.

that such more refined analysis should wait for the availability of future data with better spectral resolution and statistics.

3 DISCUSSION AND CONCLUSIONS

Evidence for small (∼30 per cent) variability in the hard X-ray component of HD 49798 was first reported by Mereghetti et al. (2011), based on the observations of 2002 September and 2008 May. Since those data were obtained at very different orbital phases, it was not clear if such variation was related to the source position in the orbit or to real long-term changes in the properties of the system. The latter possibility seems favoured by our new results, which show a ∼70 per cent flux variation between two observations spaced by six years, but taken at similar orbital phases. This suggests that the stellar wind from the hot subdwarf HD 49798, despite being much weaker than those of normal early-type stars, might be subject to time variable inhomogeneities leading to changes in the mass accretion rate, similar to those seen in high-mass X-ray binaries. The resulting luminosity variations are more prominently appearing in the harder spectral component, likely originating in shocks occurring within the accretion stream.

The new *XMM–Newton* data reported here show that the pulsar in HD 49798/RX J0648.0–4418 has continued also after 2014 its regular spin-up at the same rate of $\dot{P} = -2.17 \times 10^{-15}$ s s^{-1}. As discussed in Mereghetti et al. (2016), the mass accretion rate in this system is insufficient to cause this rapid spin-up if the compact object is a white dwarf. On the other hand, such a remarkably steady spin-up rate is difficult to explain for a neutron star subject to wind accretion: changes in the torque, resulting from variations in the stellar wind gravitationally captured by the compact object, should affect its spin period. However, no changes in $\dot{P}$ were seen, despite the observed long-term variability. These results support the intepretation of the spin-up in terms of the secular contraction of a white dwarf of few Myr age, as proposed by Popov et al. (2018).

Most of the X-ray luminosity of RX J0648.0–4418 is emitted in a soft thermal component, probably originating on the white dwarf surface. The large size of the emitting area, inferred from blackbody fits, has been one of the arguments used to disfavour a neutron star interpretation. Here, we presented the first attempt to describe this soft component with a more physical model, accounting for the presence of an atmosphere and assuming that the white dwarf is covered by helium-rich material accreted from its companion star. Fitting with this model plus a power law, we obtained reasonably good results, although the temperature could not be uniquely constrained. Remarkably, these fits result in significantly larger emission radii than those derived with the blackbody model, implying that the thermal component originates from a large fraction, or even from the totality, of the star surface.

Another relevant implication of these fits is that the contribution of the thermal emission in the UV/optical bands is much larger than that expected by the extrapolation of the best-fitting blackbody model. For example, the best atmosphere fit with $T_{eff} = 2.25 \times 10^5$ K gives an optical flux about three orders of magnitude larger than that of the blackbody. We cannot exclude that models with slightly different compositions could give an even larger flux at long wavelengths, when fitted to the X-ray data. This emission might produce detectable pulsations in the optical band, if it is modulated as strongly as in the soft X-ray band. Previous searches for optical pulsations at the spin period of 13.2 s provided an upper limit of 6×10^{-4} photons cm^{-2} s^{-1} Å^{-1} at 3600 Å (Mereghetti et al. 2011). The extrapolation of the best-fitting atmosphere model is only about one order of magnitude below this upper limit, suggesting that more sensitive searches could lead to the detection of optical pulsations or to useful constraints in case of null results.

4 SUMMARY

Because of new *XMM–Newton* observations of HD 49798/RX J0648.0–4418 carried out in 2018 and 2020, we could extend its phase-connected timing solution, now spanning a time interval of almost 30 yr, without finding any evidence of variations in the spin-up rate, despite the long-term variability in the flux of the hard X-ray component reported here for the first time.

We computed a specific white dwarf atmosphere model for this system, adopting appropriate composition and surface gravity values, and used it to describe the soft X-ray component, which was traditionally fitted with a blackbody. Our analysis showed that, in order to fully exploit the potential diagnostics of physical models of this type, data with higher spectral resolution are needed, as can be provided by future experiments such as XRISM (XRISM Science

Team 2020) and Athena/XIFU (Barret, Lam Trong & den Herder 2018). On the other hand, this first attempt indicates that atmosphere models lead to lower temperatures and much larger emission regions compared to blackbody fits. Interestingly, our best-fitting results imply that the pulsed thermal component emitted from the compact object gives a contribution in the optical/UV bands much larger than predicted by the blackbody. This opens promising prospects for future searches of optical pulsations and, more in general, for the investigation of variability in the optical band, where the contribution from the bright and hot HD 49798 is dominant.

ACKNOWLEDGEMENTS

We acknowledge financial support from INAF, through grant DP n.43/18 (Main-streams), and from the Italian Ministry for University and Research, through grant 2017LJ39LM (UNIAM). The TMAD service (http://astro-uni-tuebingen.de/~TMAD) used for this paper was constructed as part of the activities of the German Astrophysical Virtual Observatory. IP and VS were partially funded by the Deutsche Forschungsgemeinschaft (DFG) under grants GE2506/12-1 and GE2506/9-1, respectively. This work is based on data from observations with *XMM–Newton*, an ESA science mission with instruments and contributions directly funded by ESA Member States and the USA (NASA).

DATA AVAILABILITY

The data underlying this article will be shared on reasonable request to the corresponding author.

REFERENCES

Barret D., Lam Trong T., den Herder et al., 2018, in den Herder J.-W. A., Nikzad S., Nakazawa K., eds, Society of Photo-Optical Instrumentation Engineers (SPIE) Conference Series Vol. 10699, Space Telescopes and Instrumentation 2018: Ultraviolet to Gamma Ray. p. 106991G, preprint (arXiv:1807.06092)
Brooks J., Kupfer T., Bildsten L., 2017, ApJ, 847, 78
Brown A. G. A.Gaia Collaboration, et al., Gaia Collaboration, 2020, A&A, in press
Hamann W., Gruschinske J., Kudritzki R. P., Simon K. P., 1981, A&A, 104, 249
Hamann W.-R., 2010, Ap&SS, 329, 151
Heber U., 2016, PASP, 128, 082001
Israel G. L., Stella L., Angelini L., White N. E., Kallman T. R., Giommi P., Treves A., 1997, ApJ, 474, L53
Krtička J., Janík J., Krtičková I., Mereghetti S., Pintore F., Németh P., Kubát J., Vučković M., 2019, A&A, 631, A75
Kudritzki R. P., Simon K. P., 1978, A&A, 70, 653
Kurucz R. L., 2009, in Hubeny I., Stone J. M., MacGregor K., Werner K., eds, AIP Conf. Ser. Vol. 1171, Recent Directions in Astrophysical Quantitative Spectroscopy and Radiation Hydrodynamics. Am. Inst. Phys., New York, p. 43
Kurucz R. L., 2011, Canadian J. Phys., 89, 417
Mereghetti S., La Palombara N., 2016, Adv. Space Res., 58, 809
Mereghetti S., Tiengo A., Esposito P., La Palombara N., Israel G. L., Stella L., 2009, Science, 325, 1222
Mereghetti S., La Palombara N., Tiengo A., Pizzolato F., Esposito P., Woudt P. A., Israel G. L., Stella L., 2011, ApJ, 737, 51
Mereghetti S., La Palombara N., Tiengo A., Sartore N., Esposito P., Israel G. L., Stella L., 2013, A&A, 553, A46
Mereghetti S., Pintore F., Esposito P., La Palombara N., Tiengo A., Israel G. L., Stella L., 2016, MNRAS, 458, 3523
Popov S. B., Mereghetti S., Blinnikov S. I., Kuranov A. G., Yungelson L. R., 2018, MNRAS, 474, 2750
Rauch T., Deetjen J. L., 2003, in Hubeny I., Mihalas D., Werner K., eds, ASP Conf. Ser. Vol. 288, Stellar Atmosphere Modeling. Astron. Soc. Pac., San Fransisco, p. 103
Seaton M. J., Yan Y., Mihalas D., Pradhan A. K., 1994, MNRAS, 266, 805
Strüder L., Briel U., Dennerl K., et al., 2001, A&A, 365, L18
Thackeray A. D., 1970, MNRAS, 150, 215
Turner M. J. L., Abbey A., Arnaud M., et al., 2001, A&A, 365, L27
Wang B., Han Z.-W., 2010, Res. Astron. Astrophys., 10, 681
Werner K., Deetjen J. L., Dreizler S., Nagel T., Rauch T., Schuh S. L., 2003, in Hubeny I., Mihalas D., Werner K., eds, ASP Conf. Ser. Vol. 288, Stellar Atmosphere Modeling. Astron. Soc. Pac., San Fransisco, p. 31
Werner K., Dreizler S., Rauch T., 2012, Astrophysics Source Code Library, record ascl:1212.015
Wu C., Wang B., 2019, MNRAS, 486, 2977
Wu Y., Chen X., Li Z., Han Z., 2018, A&A, 618, A14
XRISM Science Team, 2020, preprint (arXiv:2003.04962)
Yungelson L. R., Tutukov A. V., 2005, Astron. Rep., 49, 871

This paper has been typeset from a TEX/LATEX file prepared by the author.